IBRACON Structures and Materials Journal
Revista IBRACON de Estruturas e Materiais
ISSN 1983-4195 ismj.org

ORIGINAL ARTICLE

Cyclic constitutive laws based on the moving focal point proposal for plain concrete under tension and compression

Leis constitutivas cíclicas baseadas na proposta de ponto focal móvel para concreto simples submetido à tensão e compressão

Lívia Ramos Santos Pereira[a]
Samuel Silva Penna[a]

[a]Universidade Federal de Minas Gerais – UFMG, Departamento de Engenharia de Estruturas, Belo Horizonte, MG, Brasil

Received 03 March 2024
Revised 15 May 2024
Accepted 19 June 2024

Abstract: This paper presents a strategy to improve the representation of the concrete response under cyclic analyses using the generalized secant modulus and the novel concept of the moving focal point. The formulated model is based on cyclic constitutive laws for plain concrete subject to cyclic compression and tension loadings. Cycles are referenced from the focal point. Linear and nonlinear approaches are proposed to reproduce the cyclic response. Numerical results for direct compression and tension simulations are compared with experimental data from the literature to validate the model. The main upgrades verified are the flexibility in reproducing load cycles and the possibility of correlating the numerical curve to the physical parameters of concrete. The contribution of this study is the moving focal point concept, a strategy to better adjust cyclic paths compared to the fixed focal point.

Keywords: concrete, cyclic load, constitutive laws, moving focal point.

Resumo: Esse artigo apresenta uma estratégia para aprimorar a representação da resposta do concreto submetido a análises cíclicas utilizando o módulo secante generalizado e o novo conceito de ponto focal móvel. A formulação do modelo é baseada em leis constitutivas cíclicas para o concreto simples sob compressão ou tração cíclica. Os ciclos têm como referência o ponto focal móvel. Abordagens linear e não linear são propostas para reproduzir a resposta cíclica. Os resultados numéricos das simulações de compressão e tração diretas são comparados com dados experimentais da literatura para validar o modelo. As principais melhorias verificadas são a flexibilidade em reproduzir ciclos de carga e a possibilidade de correlacionar a curva numérica a parâmetros físicos do concreto. A contribuição deste estudo é o conceito de ponto focal móvel, uma estratégia com melhor ajuste que o ponto focal fixo.

Palavras-chave: concreto, carga cíclica, leis constitutivas, ponto focal móvel.

How to cite: L. R. S. Pereira and S. S. Penna, "Cyclic constitutive laws based on the moving focal point proposal for plain concrete under tension and compression," *Rev. IBRACON Estrut. Mater*., vol. 17, no. 2, e17212, 2024, https://doi.org/10.1590/S1983-41952024000200012

1 INTRODUCTION

The computational study of concrete structures demands constitutive models to reproduce the behavior of this complex material. Considering cyclic loadings, unloading-reloading strategies are required. Although the cyclic concrete response is not a recent research field, the contemporary context has encouraged new studies in this area due to the evolution of computational methods.

Sinha et al. [1] developed the first paper published about concrete hysteretic behavior. The authors performed a series of experiments to describe the stress-strain response of concrete cylinders subjected to cyclic axial compressive loadings. From these tests, they derived stress-strain laws for cyclic loading.

Corresponding author: Lívia Ramos Santos Pereira. E-mail: lrsp@ufmg.br
Financial support: Brazilian research agency CNPq (in Portuguese Conselho Nacional de Desenvolvimento Científico e Tecnlógico) – PhD Scholarship and the Research Grant n. 307985/2020-2.
Conflict of interest: Nothing to declare.
Data Availability: The data that support the findings of this study are available from the corresponding author, LRSP., upon request.

This is an Open Access article distributed under the terms of the Creative Commons Attribution License, which permits unrestricted use, distribution, and reproduction in any medium, provided the original work is properly cited.

Karsan and Jirsa [2] also conducted an experimental study of plain concrete under cyclic compression. The authors proposed an empirical formula based on the residual plastic strain, which defines where the unloading process starts, to determine the envelope and the unloading and reloading stress-strain curves. The results showed that the cyclic paths usually respect the envelope curve.

After this, many models for cyclic behavior were proposed. Some of these models are based on the theory of elasticity, others come from the continuum damage mechanics, and others are derived from plasticity. In addition to the classic approaches, simplified models try to generalize experimental results from mathematical relationships [3]–[6].

Yankelevsky and Reinhardt [5] proposed the focal points model for the uniaxial cyclic behavior of concrete. This model determines points that govern the unloading-reloading curves in the softening branch. It is a graphical method where the coordinates of the focal points are functions of the envelope parameters, being different for each cycle.

Lee et al. [7] and Lee and Willam [8] introduced the focal point concept to analyze unloading-reloading paths of concrete under uniaxial compression. Determining a fixed point to direct the cycles was a representation resource for both the stiffness reduction and the plastic strains. These authors have considered a unique focal point with coordinates based on experimental observation. The loops were simplified by lines. Afterward, Kwon and Spacone [9] adopted the focal point as the tensile strength coordinates to orientate load cycles in concrete under compressive stresses.

During the last years, numerous concrete models for cyclic loadings have been proposed due to the development of computational methods. The focal point concept, however, has been overlooked. Alva et al. [10] proposed a numerical model based on the Lumped Damage Mechanics (LDM), considering two scalar variables to represent the nonlinear behavior of reinforced concrete: a damage variable related to concrete cracking and a plastic rotation to quantify the steel bar yielding. Breccolotti et al. [11] improved the model of Sima et al. [12] to describe damage accumulation better and extended the method to high-strength concrete. A model able to capture the crack opening and closing was proposed by Moharrami and Koutromanos [13], combining plasticity and a smeared crack model. Feng et al. [14] focused on developing a damage model to precast concrete under cyclic loading.

Recently, Pereira and Penna [15] rescued the application of a fixed focal point to conduct hysteretic analyses. These authors highlighted that such a strategy conducted better results than other approaches to reproduce load cycles, such as the elastic and secant approaches. They also verified that the focal point coordinates strongly affect the cycle configuration, suggesting the development of a more accurate methodology to define this pole.

Although some studies have been motivated by the focal point determination, this concept has not been fully explored. The present paper analyzes the focal point, its uses, and limitations. A new approach is also proposed to embrace the simplicity of the model presented in Lee et al. [7] and Lee and Willam [8] and the representation flexibility from [4]–[6] using a moving focal point. Numerical examples of cyclic tension and cyclic compression are performed to evaluate the improvements in the loop representation using a moving focal point instead of a fixed focus.

2 CYCLIC CONSTITUTIVE MODEL

The behavior of quasi-brittle materials such as concrete starts from describing the nucleation and propagation of smeared and discrete cracks in the material media. Two hypotheses to characterize this process are highlighted: the first considers the crack as a discontinuity of the material media, representing it from discretization; the second assumes the smeared aspect of concrete cracking, admitting the degradation of material properties.

From the phenomenological approach, the smeared models represent cracking according to the elastic modulus degradation. Stress-strain laws and generalized constitutive relationships are required to reproduce the behavior of material points. Initial studies of smeared crack models [16]–[21] established that the material degradation represents the evolution of cracks caused by the loads as a function of a strain measure and constitutive relationships.

This work presents a smeared crack model for concrete based on Rots [20] and Rots et al. [21] that evaluates the elastic modulus degradation in a local system of cracks, defined from the principal strain directions, and considers experimental evolution laws. This model has as a hypothesis that, before cracking, the material is homogeneous, continuous, linear, elastic, and isotropic. After cracking, the homogeneity and continuity of the medium are preserved, but the material becomes nonlinear, inelastic, and orthotropic.

Thus, nonlinearity is introduced in the model through stress-strain relations. The inelastic regime is controlled by resistance limits and material fracture energy, while an appropriate constitutive tensor represents the orthotropy. The generalized constitutive relation in the material local orthotropy system can be written as Equation 1

$$\{\sigma_\ell\} = [\mathrm{D}_\ell^{\mathrm{s}}]\{\varepsilon_\ell\}, \tag{1}$$

where $\{\sigma_\ell\}$ is the local stress tensor, $[D_\ell^s]$ is the constitutive secant tensor in the local system, and $\{\varepsilon_\ell\}$ is the local strain tensor. The first-order tensors are represented by $\{.\}$, while $[.]$ is used for second-order tensors.

Although the constitutive secant tensor of Equation 1 is defined for the local cracking system, the constitutive relations in the global system are required in computational modeling by the Finite Element Method, which is obtained as Equation 2

$$\{\sigma_\ell\} = [T_\sigma]\{\sigma_g\}, \tag{2}$$

where $\{\sigma_g\}$ is the global stress tensor and $[T_\sigma]$ is the stress transformation tensor. Similarly, for the strains, the relation is represented by Equation 3

$$\{\varepsilon_\ell\} = [T_\varepsilon]\{\varepsilon_g\}. \tag{3}$$

Replacing Equation 2 and Equation 3 in the relationship between local stresses and strains (Equation 1), it is given Equation 4

$$[T_\sigma]\{\sigma_g\} = [D_\ell^s][T_\varepsilon]\{\varepsilon_g\}. \tag{4}$$

Since $[T_\sigma] = [T_\varepsilon]^{-T}$, σ_g can be represented by Equation 5

$$\{\sigma_g\} = [T_\varepsilon]^T[D_\ell^s][T_\varepsilon]\{\varepsilon_g\}. \tag{5}$$

Rewriting Equation 5, it is expressed for Equation 6

$$\{\sigma_g\} = [D_g^s]\{\varepsilon_g\}, \tag{6}$$

where the constitutive secant tensor in the global system is (Equation 7)

$$[D_g^s] = [T_\varepsilon]^T[D_\ell^s][T_\varepsilon]. \tag{7}$$

In a nonlinear solution method, as Standard Newton-Raphson, the constitutive tangent operator must be defined. Considering the stress transformation (Equation 2), it is calculated as Equation 8

$$\{\sigma_g\} = [T_\sigma]^{-1}\{\sigma_\ell\}, \tag{8}$$

or, in terms of strain transformation (Equation 9)

$$\{\sigma_g\} = [T_\varepsilon]^T\{\sigma_\ell\}. \tag{9}$$

Deriving Equation 9 in relation to ε_g, it is given Equation 10

$$\frac{\partial\{\sigma_g\}}{\partial\{\varepsilon_g\}} = \frac{\partial}{\partial\varepsilon_g}([T_\varepsilon]^T\{\sigma_\ell\}). \tag{10}$$

Developing Equation 10, it can be expressed as Equation 11

$$\frac{\partial\{\sigma_g\}}{\partial\{\varepsilon_g\}} = [T_\varepsilon]^T\frac{\partial\{\sigma_\ell\}}{\{\varepsilon_g\}} + \frac{\partial[T_\varepsilon]^T}{\{\varepsilon_g\}}\{\sigma_\ell\}, \tag{11}$$

that can be rewritten as Equation 12

$$\frac{\partial\{\sigma_g\}}{\partial\{\varepsilon_g\}} = [T_\varepsilon]^T\frac{\partial\{\sigma_\ell\}}{\partial\{\varepsilon_\ell\}}\frac{\partial\{\varepsilon_\ell\}}{\partial\{\varepsilon_g\}} + \frac{\partial[T_\varepsilon]^T}{\partial\{\varepsilon_g\}}\{\sigma_\ell\}. \tag{12}$$

Considering $[T_\varepsilon] = \frac{\partial\{\varepsilon_\ell\}}{\partial\{\varepsilon_g\}}$, it is given Equation 13

$$\frac{\partial\{\sigma_g\}}{\partial\{\varepsilon_g\}} = [T_\varepsilon]^T\frac{\partial\{\sigma_\ell\}}{\partial\{\varepsilon_\ell\}}[T_\varepsilon] + \frac{\partial[T_\varepsilon]^T}{\partial\{\varepsilon_g\}}\{\sigma_\ell\}, \tag{13}$$

where Equation 14

$$[D_\ell^t] = \frac{\partial\{\sigma_\ell\}}{\partial\{\varepsilon_\ell\}} \tag{14}$$

is the local constitutive tangent tensor. Then, Equation 13 can be expressed as (Equation 15):

$$\frac{\partial\{\sigma_g\}}{\partial\{\varepsilon_g\}} = [T_\varepsilon]^T[D_\ell^t][T_\varepsilon] + \frac{\partial[T_\varepsilon]^T}{\partial\{\varepsilon_g\}}\{\sigma_\ell\}, \tag{15}$$

where $\frac{\partial[T_\varepsilon]^T}{\partial\{\varepsilon_g\}}\{\sigma_\ell\}$ represents the transformation tensor variation relating to global strains.

The relation given in Equation 14 is the local tangent constitutive tensor, where $\frac{\partial\{\sigma_\ell\}}{\partial\{\varepsilon_\ell\}}$ is obtained by deriving Equation 1, resulting in Equation 16

$$[D_\ell^t] = \frac{\partial\{\sigma_\ell\}}{\partial\{\varepsilon_\ell\}} = [D_\ell^s] + \frac{\partial\{D_\ell^s\}}{\partial\{\varepsilon_\ell\}}\{\varepsilon_\ell\}, \tag{16}$$

where D_ℓ^s is the local secant tensor and $\frac{\partial[D_\ell^s]}{\partial\{\varepsilon_\ell\}}\{\varepsilon_\ell\}$ represents the constitutive tensor variation due to the evolution of the local strains.

The dependent term on the direction variation of the local system, oriented to θ, is given by Equation 17

$$\frac{\partial[T_\varepsilon]^T}{\partial\{\varepsilon_g\}}[\sigma_\ell] = \frac{\partial[T_\varepsilon]^T}{\partial\theta}\{\sigma_\ell\}\frac{\partial\theta}{\partial\{\varepsilon_g\}}, \tag{17}$$

which is symmetric if there is coaxially between principal stresses and strains.

Equation 15 can be rewritten in terms of Equations 16 and 17, as Equation 18

$$\frac{\partial\{\sigma_g\}}{\partial\{\varepsilon_g\}} = [T_\varepsilon]^T[D_\ell^t][T_\varepsilon] + \frac{\partial[T_\varepsilon]^T}{\partial\theta}\{\sigma_\ell\}\frac{\partial\theta}{\partial\{\varepsilon_g\}}, \tag{18}$$

where the global tangent tensor is represented by Equation 19

$$[D_g^t] = \frac{\partial\{\sigma_g\}}{\partial\{\varepsilon_g\}}. \tag{19}$$

Replacing Equation 16 in Equation 18, it can be written Equation 20

$$[D_g^t] = [T_\varepsilon]^T\left([D_\ell^s] + \frac{\partial[D_\ell^s]}{\partial\{\varepsilon_\ell\}}\{\varepsilon_\ell\}\right)[T_\varepsilon] + \frac{\partial[T_\varepsilon]^T}{\partial\theta}\{\sigma_\ell\}\frac{\partial\theta}{\partial\{\varepsilon_g\}}. \tag{20}$$

Traditionally, smeared crack models can assume two hypotheses for crack propagation. The first hypothesis establishes that the cracking direction is rotational, varying according to the principal strains, which is represented by the portion $\partial\theta/\partial\{\varepsilon_g\}$ of the tangent operator. The second hypothesis assumes that the propagation direction remains fixed as the direction of the principal strain system at the moment of nucleation. In this last case, the part associated with the variation of the directions is null $\left(\partial\theta/\partial\{\varepsilon_g\} = 0\right)$, simplifying the tangent operator to Equation 21

$$[D_g^t] = [T_\varepsilon]^T[D_\ell^t][T_\varepsilon]. \tag{21}$$

For a plane stress analysis, the adopted secant constitutive tensor in matrix format is shown in Equation 22:

$$[D_\ell^s] = \frac{1}{1-\frac{\psi}{E_0}\nu}\begin{bmatrix} E_1(\varepsilon_1) & \psi & 0 \\ \psi & E_2(\varepsilon_2) & 0 \\ 0 & 0 & \left(1-\frac{\psi}{E_0}\nu\right)G_{12}(\varepsilon_1,\varepsilon_2) \end{bmatrix}, \tag{22}$$

With ψ given by Equation 23

$$\psi = \frac{E_1(\varepsilon_1)E_2(\varepsilon_2)\nu}{E_0}, \tag{23}$$

and E_0 as the elastic modulus of the material, ν as the Poisson coefficient, $E_1(\varepsilon_1)$ and $E_2(\varepsilon_2)$ as the secant modules written as a function of the principal strains.

The evolution of the secant modulus can be calculated from stress-strain laws for concrete, such as Carreira and Chu's [22] law for compression (Figure 1a), expressed by Equation 24:

$$\sigma(\varepsilon) = f_c\,\frac{K_c\,(\varepsilon/\varepsilon_c)}{K_c-1+(\varepsilon/\varepsilon_c)^{K_c}}, \tag{24}$$

where f_c is the compressive strength of the concrete, ε_c is the strain associated with f_c, and K_c is given by Equation 25

$$K_c = \frac{1}{1-\left(\frac{f_c}{\varepsilon_c}\frac{1}{E_0}\right)}. \tag{25}$$

For tension, there are relationships such Boone and Ingraffea [23] law (Figure 1b), defined by Equation 26:

$$\sigma(\varepsilon) = f_t \cdot e^{-K_t(\varepsilon-\varepsilon_t)}, \tag{26}$$

where f_t is the tensile strength of concrete, $\varepsilon_t = f_t/E_0$, and K_t is calculated as Equation 27

$$K_t = \frac{h \cdot f_t}{G_f}. \tag{27}$$

Where h is the characteristic length, and G_f is the fracture energy of concrete.

The shear modulus is related to the longitudinal modulus, given by Equation 28

$$G_{12}(\varepsilon_1, \varepsilon_2) = \frac{E_0 E_1(\varepsilon_1) E_2(\varepsilon_2)}{E_0 E_1(\varepsilon_1) + E_0 E_2(\varepsilon_2) + 2\nu E_1(\varepsilon_1) E_2(\varepsilon_2)}, \tag{28}$$

In the local tangent operator (Equation 16), the variation of the constitutive tensor with strain evolution is given by Equation 29:

$$\frac{\partial[D_\ell^s]}{\partial\{\varepsilon_\ell\}}\{\varepsilon_\ell\} = \begin{bmatrix} \frac{\partial_\ell^s D_{11}}{\partial\varepsilon_1}\varepsilon_1 + \frac{\partial_\ell^s D_{12}}{\partial\varepsilon_1}\varepsilon_2 & \frac{\partial_\ell^s D_{11}}{\partial\varepsilon_2}\varepsilon_1 + \frac{\partial_\ell^s D_{12}}{\partial\varepsilon_2}\varepsilon_2 & 0 \\ \frac{\partial_\ell^s D_{12}}{\partial\varepsilon_1}\varepsilon_1 + \frac{\partial_\ell^s D_{22}}{\partial\varepsilon_1}\varepsilon_2 & \frac{\partial_\ell^s D_{12}}{\partial\varepsilon_2}\varepsilon_1 + \frac{\partial_\ell^s D_{22}}{\partial\varepsilon_2}\varepsilon_2 & 0 \\ 0 & 0 & 0 \end{bmatrix}, \tag{29}$$

where D_{11}, D_{12}, $D_{21}$and D_{22} are the constitutive tensor terms of Equation 22.

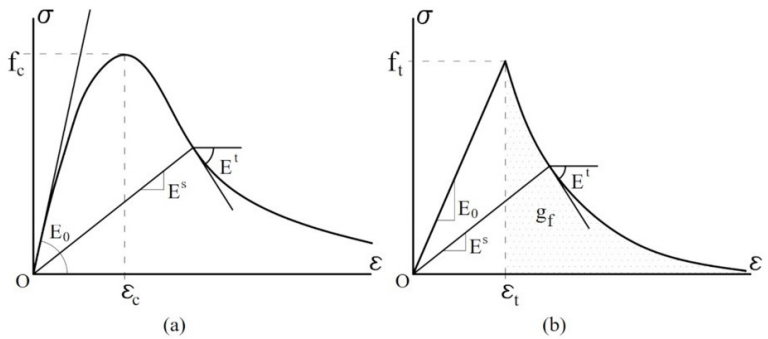

Figure 1. Stress-strain laws for concrete under compression (a) and tension (b).

To complete the tangent operator, considering the plane stress state, the strain transformation matrix is written as Equation 30

$$[T_\varepsilon] = \begin{bmatrix} \cos^2\theta & \sin^2\theta & \cos\theta\sin\theta \\ \sin^2\theta & \cos^2\theta & -\cos\theta\sin\theta \\ -2\cos\theta\sin\theta & 2\cos\theta\sin\theta & \cos^2\theta - \sin^2\theta \end{bmatrix}, \tag{30}$$

whose derivative related to θ is Equation 31

$$\frac{\partial[T_\ell]^T}{\partial\theta} = \begin{bmatrix} -2\cos\theta\sin\theta & 2\cos\theta\sin\theta & -2(\cos^2\theta - \sin^2\theta) \\ 2\cos\theta\sin\theta & -2\cos\theta\sin\theta & 2(\cos^2\theta - \sin^2\theta) \\ \cos^2\theta - \sin^2\theta & -(\cos^2\theta - \sin^2\theta) & -4\cos\theta\sin\theta \end{bmatrix}. \tag{31}$$

The principal strain directions are defined by θ and the axes 1 and 2, while xy is the global system (Figure 2). This angle can be calculated as Equation 32:

$$\tan 2\theta = \frac{\gamma_{xy}}{\varepsilon_x - \varepsilon_y} \therefore \theta = \frac{1}{2}\arctan\left(\frac{\gamma_{xy}}{\varepsilon_x - \varepsilon_y}\right). \tag{32}$$

Therefore, its derivative (Equation 33) is calculated concerning the strains $\{\varepsilon_g\}$, which can be seen in Equation 20. Then

$$\frac{\partial\theta}{\partial\{\varepsilon_g\}} = \frac{1}{2}\frac{\gamma_{xy}}{(\varepsilon_x-\varepsilon_y)^2+\gamma_{xy}^2}\begin{bmatrix}-1\\1\\\frac{\varepsilon_x-\varepsilon_y}{\gamma_{xy}}\end{bmatrix}. \tag{33}$$

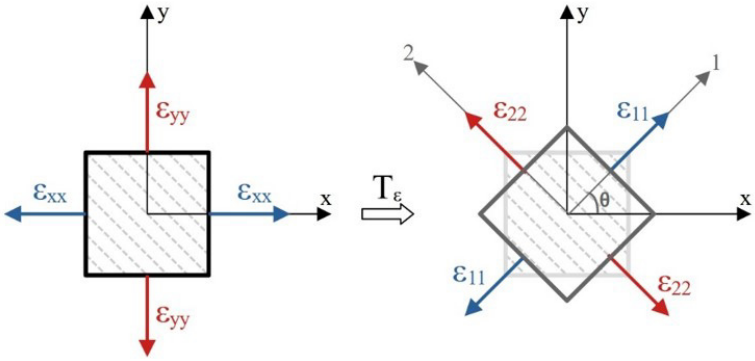

Figure 2. Principal strain directions and the global system.

In the presented model, it is possible to adopt different forms for the constitutive tensor and different laws of evolution. Such features are relevant in cyclic analyses where stress-strain laws are required to represent load cycles.

For the cyclic analysis, in addition to material evolution laws, the secant modules $E_1(\varepsilon_1)$ and $E_2(\varepsilon_2)$, presented in the constitutive tensor of Equation 22, are replaced by the modules of unloading or reloading. In this work, the unloading and reloading modules are obtained from the generalized secant modulus (section 3). Finally, the control of the cycles is established by the loading functions. For a plane stress state, two functions are needed (Equations 34 and 35)

$$f_1 = \varepsilon_1 - \kappa(\varepsilon_1), \tag{34}$$

$$f_2 = \varepsilon_2 - \kappa(\varepsilon_2), \tag{35}$$

where ε_1 and ε_2 are the principal strains, and $\kappa(\varepsilon_1)$ and $\kappa(\varepsilon_2)$ are the historical variables (Equations 36 and 37)

$$\kappa(\varepsilon_1) = \max_{0\le s\le t}\{\varepsilon_1(s)\}, \tag{36}$$

$$\kappa(\varepsilon_2) = \max_{0\le s\le t}\{\varepsilon_2(s)\}. \tag{37}$$

Thus, the load regime is defined according to

Elastic loading $\rightarrow f < 0;\ \dot{f} > 0; \kappa = \kappa_0;\ \dot{\kappa} = 0.$

Loading with degradation $\rightarrow f = 0;\ \dot{f} = 0; \kappa > \kappa_0;\ \dot{\kappa} > 0.$

Unloading $\rightarrow f < 0;\ \dot{f} < 0; \kappa > \kappa_0;\ \dot{\kappa} = 0.$

Reloading $\rightarrow f < 0;\ \dot{f} > 0; \kappa > \kappa_0;\ \dot{\kappa} = 0.$

3 CYCLIC STRESS-STRAIN LAWS BASED ON A FIXED FOCUS

The smeared crack models require stress-strain relations to represent the real behavior of a material and its degradation. These stress-strain laws must be complete to reproduce the concrete response under cyclic loadings, representing the envelope curve and the unloading-reloading paths. There is a wide variety of monotonic curve proposals in the literature, and it is well-known that they apply to cyclical analyses to represent the envelope curve. The cyclic paths, although, still need to be discussed.

3.1 Linear approach based on a fixed focal point

Lee and Willam [8] proposed a procedure based on experimental observation and three energy mechanisms to find the focal point: residual strain, damage, and elastic deformation. Regarding the focal point coordinates, the authors adopt a unique focal point to describe stiffness degradation.

A computational procedure based Lee et al. [7] and Lee and Willam [8] is developed to simulate linear unloading-reloading paths referenced from a focal point. The method is pictured in Figure 3a, where the line defined by the focal point $(\varepsilon_f, \sigma_f)$ and the unloading point $(\varepsilon_u, \sigma_u)$ is a simplified representation of the hysteresis cycle, and ε^e is the elastic strain and ε^p the permanent strain.

The initial step is to determine the generalized secant modulus (E_{SG}), given by Equation 38:

$$E_{SG} = \frac{\sigma'}{\varepsilon'}, \tag{38}$$

where $\varepsilon'$and σ' are coordinates of a point that belongs to the unloading-reloading path.

The linear modulus (E_L), which is the slope of the line representing the load cycle, can be used to obtain σ'. This slope is calculated as Equation 39:

$$E_L = \frac{\Delta\sigma}{\Delta\varepsilon} = \frac{\sigma_u - \sigma_f}{\varepsilon_u - \varepsilon_f} = \frac{\sigma_u - \sigma'}{\varepsilon_u - \varepsilon'}. \tag{39}$$

Equation 39 can be rewritten to define the current stress at the cycle path, as Equation 40:

$$\sigma' = \sigma_u - \left(\frac{\sigma_u - \sigma_f}{\varepsilon_u - \varepsilon_f}\right)(\varepsilon_u - \varepsilon'). \tag{40}$$

The E_{SG} can also be associated with other cyclic curves with different shapes.

3.2 Nonlinear approach based on a fixed focal point

Nevertheless, the linear approach is a simplification of unloading-reloading paths. Li and Ren [24] emphasize that studies indicate that concrete presents a curve-shaped hysteresis loop when subjected to compressive loads. A nonlinear approach is described to cover these cases. The uniaxial law proposed in Balan et al. [25] and improved in Kwon and Spacone [9] and Balan et al. [26] combines the curve of Popovics [27] before the peak of compressive stress with the curve of Saenz [28] after the peak. The concrete compression behavior under monotonic loading is given by Equation 41

$$\sigma = f_c \frac{K(\varepsilon/\varepsilon_c)}{1 + A(\varepsilon/\varepsilon_c) + B(\varepsilon/\varepsilon_c)^2 + C(\varepsilon/\varepsilon_c)^3 + D(\varepsilon/\varepsilon_c)^R}, \tag{41}$$

where
$K = E^0(\varepsilon_c/f_c)$; $R = K/(K-1)$; f_c is the compressive strength; ε is the current strain; ε_c is the strain associated with f_c ; and A, B, C, D are variables that depend on whether the branch is ascending or descending.

Ascending branch [27]:

$$(\varepsilon/\varepsilon_c) \leq 1: A = C + K - 2;\ B = 1 - 2; C = K\left(\frac{K_\sigma - 1}{K_\varepsilon - 1}\right) - \frac{1}{K_\varepsilon}; D = 0.$$

Descending branch [28]:

$$(\varepsilon/\varepsilon_c) > 1: A = B = C = 0; D = (K - 1).$$

The variables K_σ and K_ε are adjustment parameters (Equations 42 and 43) that relate the peak with a control point coordinates in the descending branch $(\varepsilon_p, \sigma_p)$:

$$K_\varepsilon = \varepsilon_p/\varepsilon_c, \tag{42}$$

$$K_\sigma = f_c/\sigma_p. \tag{43}$$

To extend this stress-strain law to cyclic analyses, Bono and Campos [29] adapted the monotonic curve of Equation 41. For the unloading process, the origin of the curve becomes the point $(\varepsilon_u, \sigma_u)$, where unloading starts, and the peak is replaced by the focal point $(\varepsilon_f, \sigma_f)$. For reloading, the origin is given by the coordinates $(\varepsilon_r, \sigma_r)$, where reloading begins, and the peak is replaced by the unloading point $(\varepsilon_u, \sigma_u)$. This nonlinear cyclic approach is illustrated in Figure 3b, where ε_{max} is the maximum strain experimentally observed.

These authors adopted the proposal of Kwon and Spacone [9] to establish the focal point coordinates: the focus coincides with the tensile strength point when the structure is under compressive loads, while the focal point is the compression strength for a tensile load.

4 CYCLIC STRESS-STRAIN LAWS BASED ON MULTIPLE FOCUSES

The major drawback of the fixed focal point is that some cycles can be appropriately represented, while others may present a poor approximation compared to experimental data. Yankelevsky and Reinhardt [4]–[6] addressed the multiple focal points theory based on experimental observations.

The samples analyzed in Yankelevsky and Reinhardt [4]–[6] indicated that, for both tension and compression load, the unloading paths presented stiffness degradation and also permanent strains. For compressive loads, more pronounced unloading occurs when the cycle starts at a larger strain, as though all unloading curves are directed to a low strain point [4]. For tensile loads, the loops are closer and narrower at a low strain level [6].

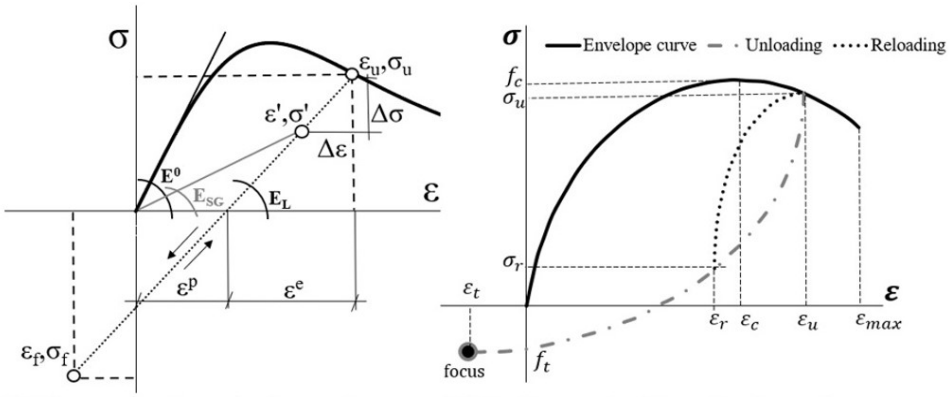

Figure 3. Cyclic approaches based on a fixed focal point.

Then, based on the different behaviors observed on the hysteresis loops, the authors proposed multiple focal points whose coordinates are defined according to the envelope curve parameters. This approach is more representative since the unloading-reloading path configuration depends on the strain level observed where the cycle starts.

The compression model, indicated in Figure 4a, demands six focal points, C_1 to C_6 [5]. The first five points are located in the tangent line to the monotonic curve in its elastic stretch. The sixth point is on the strain axis. The points $C_1 - C_6$ stress coordinates are related to concrete compression strength, as indicated in Table 1. As illustrated in Figure 4a, ε_0, is the strain associated with the stress peak. The unloading starts at point A, and its path is determined by linear stretches that connect A-C-D-B. The reloading is defined by the path B-C-K. The coordinates of A, B, C, D, and K are given in Yankelevsky and Reinhardt [4].

On the other hand, the tensile model (Figure 4b) defines seven focal points [5]. The first one is the origin (T_0). The points $T_1 - T_5$ are located in the monotonic curve tangent at the origin. And the point T_6 coordinates depend on the strain where the unloading starts (ε_A), given as $[0.5\,\varepsilon_A;\ -0.075\,f_t]$. The stress coordinates of $T_0 - T_5$ are associated with concrete tensile strength and are presented in Table 1. The unloading path is compounded by linear stretches among the points A-C-D-B, and, in case of stress sign inversion, it is prolonged to B-E-F-G. The reloading follows the path G-H-I-J-K-M. These points coordinates are explicit in [6].

However, the multiple focal points theory has a geometric appeal and many empirical estimates. These features limit its implementation in a computational environment. Another restriction is about the unloading-reloading path reproduction. A set of lines simplifies them, and when nonlinearity is relevant, this approach demands improvements. Because of these drawbacks, this paper presents a proposal that embraces the flexibility of working with different focal points and is also more automated and adequate for computational analyses.

Table 1. Focal points stress coordinates.

Point	Coordinate	Point	Coordinate	Point	Coordinate
C_1	$3f_c$	C_2	f_c	C_3	$0.75f_c$
C_4	$0.47f_c$	C_5	$0.2f_c$	C_6	$0.0; \varepsilon = \varepsilon_0$
T_0	0.0	T_1	$-3f_t$	T_2	$-f_t$
T_3	$-0.75f_t$	T_4	$-0.5f_t$	T_5	$-0.125f_t$

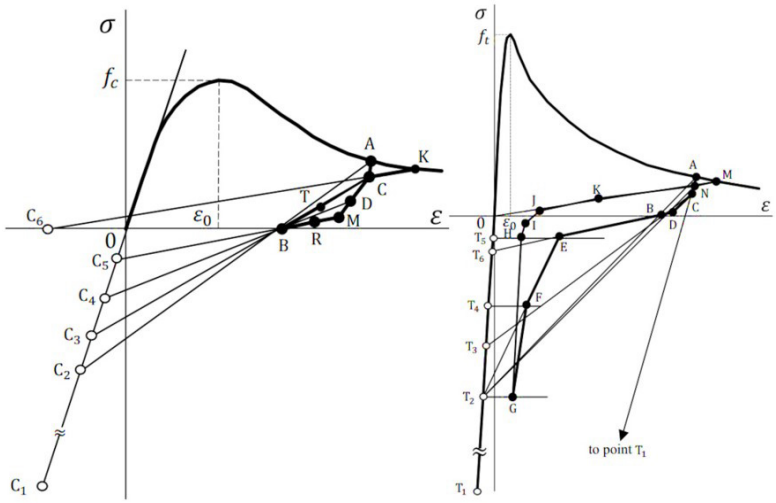

Figure 4. Model based on multiple focal points (adapted from Yankelevsky and Reinhardt [5]).

5 CYCLIC STRESS-STRAIN LAWS BASED ON A MOVING FOCAL POINT

Based on the studies previously described, an unloading-reloading strategy is proposed, considering a moving focal point. This strategy starts by generalizing the multiple focal points. The focal point is calculated at runtime to associate the load loops with the current degradation state of the elastic modulus. This proposal is combined with the generalized secant modulus to allow the stiffness matrix calculus and the cycle reproduction.

Two models grounded in stress-strain laws are developed to reproduce load cycles better. The novelty of these models is the adoption of a moving focal point. The two approaches differ because the first model represents the cycles using a line, with coincident unloading and reloading paths, while the second model admits a nonlinear unloading-reloading law.

5.1 Linear approach based on a moving focal point

The linear approach is developed by a relation that calculates the elastic modulus degradation and, consequently, the permanent strain. This calculus comes from a proportion between the strain value where starts a cycle i (ε_{ui}) and a maximum strain ε_{max}. This maximum strain is initially adopted as the maximum strain observed in the experimental analyses, and it can be modified to adjust the load cycles better.

During the first unloading, the elastic modulus (E^0) defines the path. The intersection point between this path and the strain axis is the reference focal point strain (ε_{ref}). In the subsequent cycles, a degradation percentage (P_{di}) is estimated by a linear relation (Equation 44):

$$P_{di} = \frac{\varepsilon_{max} - \varepsilon_{ui}}{\varepsilon_{max} - \varepsilon_{ref}}, \tag{44}$$

where i is the cycle number. The damaged modulus in the current cycle is obtained from Equation 45:

$$E_{ui} = P_{di} \cdot E^0. \tag{45}$$

The proposed methodology is illustrated in Figure 5a. Such an approach is adopted to describe compression and tensile loads. The stiffness degradation and the permanent strain are two crescent quantities because the material cannot recover its mechanical properties. To guarantee the previous formulation (Equations. 44 and 45) agrees with these requirements, two strategies should be applied.

In the first strategy (Figure 5b), if the current strain degradation is inferior to the previous one, the permanent strain of the current cycle is fixed as the previous one. Such a procedure avoids a false result, represented by the continuous lines in Figure 5b, which is replaced by a plausible response, represented by the dashed lines.

In the second strategy (Figure 5c), when the permanent strain associated with the current cycle is inferior to the previous one, the current damaged modulus is established as the last loop hysteresis. The aim of this technique is the same as the first strategy, but different parameters are used. The advantage of having two possibilities is reaching a better adjustment between the numerical and the experimental curve. Figure 5c presents the results without using such strategies in continuous lines, while dashed lines represent the cycles after E fixation.

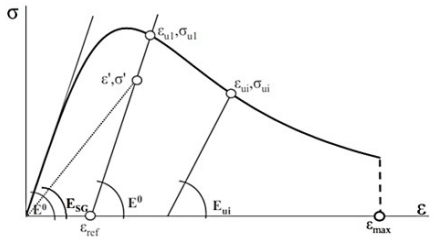

(a) Stress-strain law with moving focal point and linear unloading-reloading.

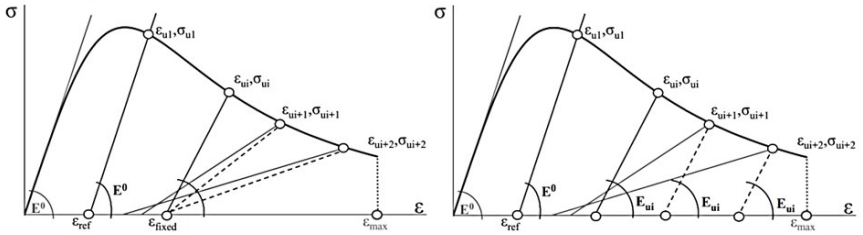

(b) Correction strategy: ε fixed. (c) Correction strategy: E fixed.

Figure 5. Stress-strain law with moving focal point and linear unloading-reloading.

5.2 Nonlinear approach based on a moving focal point

The nonlinear approach is developed considering the aforementioned unloading-reloading paths and generalizing the multiple focus proposal. The intention of coupling these theories is to adapt this methodology to computational analyses, resulting in a representative and automated model to reproduce experimental data.

The tensile model has three auxiliary points (T_2, T_4, T_5), and the stress intervals that delimit these points are used to locate the unloading stress of a specific cycle (σ_u). These intervals are related to the concrete tensile strength, f_t, and their limits are listed in Table 2.

Thus, the focal points can be determined as indicated in Figure 6a. These points are the intersection between the line that goes through the point where the unloading starts and the respective auxiliary point ($T_2, T_4,$ or T_5) and the strain axis. Once the focal point of the cycle is located, the unloading and the reloading curve are described by the law of section 3.2.

The compression model follows a similar methodology to the tensile model, adopting the auxiliary points C_2, C_4, and C_5. These points depend on the compression strength of the concrete (f_c) and are correlated to stress intervals. Further, the unloading stress, σ_u, determines which auxiliary point will be admitted. The stress intervals and the associated points are summarized in Table 2.

Table 2. Relation among the auxiliaries points and the stress intervals.

Condition	σ_{aux}	ε_{aux}	Auxiliary point
$\sigma_u > 0.75\ f_t$	$-f_t$	$-f_t/E^0$	T_2
$0.75\ f_t > \sigma_u > 0.25\ f_t$	$-0.5f_t$	$-0.5f_t/E^0$	T_4
$\sigma_u < 0.75\ f_t$	$-0.125f_t$	$-0.125f_t/E^0$	T_5
$\sigma_u > 0.75\ f_c$	$-f_c$	$-f_c/E^0$	C_2
$0.75\ f_c > \sigma_u > 0.375\ f_c$	$-0.47f_c$	$-0.47f_c/E^0$	C_4
$\sigma_u < 0.375\ f_c$	$-0.2f_c$	$-0.2f_c/E^0$	C_5

The auxiliary points and the unloading stress guide the process that determines the focal points in the same way as the tensile model. This methodology is represented in Figure 6b.

Some observations of [5] are also included in the proposed models. As shown in Figure 4, point B intercepts the strain axis. Since this point represents a physical parameter, the permanent strain, it was considered essential, so point B was adopted as the focal point of the proposed models.

The points K, for compression, and M, for tensile (Figure 4), also deserve attention. They indicate that the reloading path does not converge to the unloading stress but to a point ahead of the envelope curve. Based on this observation, a parameter was included in the proposed models: the increment of the historical variable $\Delta\kappa$. This variable defines how many times the strain at the final reloading point is larger than ε_u.

A study was conducted to establish a consistent value interval for $\Delta\kappa$, based on 11 experiments from the literature: seven compression and four tensile tests. These data are available in [4]–[6], but the authors who performed the experiments are [1]–[3], [30]–[35]. Considering this analysis, $\Delta\kappa$ generally lies between 1.01 and 1.30 (Table 3).

The stress-strain law from Popovics-Saenz and adapted to cyclic loads for [29] also had its parameters evaluated, aiming to adjust experimental results better. By varying these parameters in a spreadsheet, it was observed that the exponent R (Equation 41) is decisive in the cycle configuration. Then, two adjustment variables for the R factor were created, the first for unloading and the second for reloading. These variables can assume values from 0 to 1, representing a percentage that R must be multiplied, as illustrated in Figure 7. Values closer to zero lead to less pronounced curvature, while values closer to 1 intensify the path circular shape.

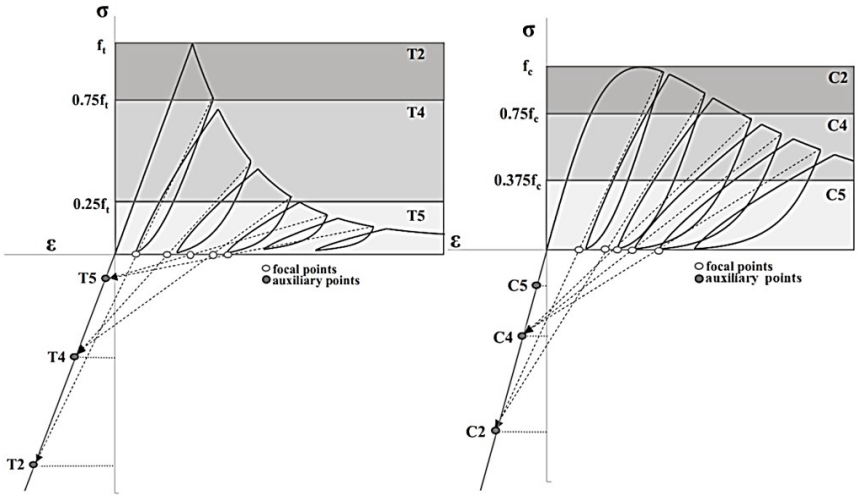

(a) Tensile model. (b) Compression model.

Figure 6. Nonlinear cyclic approach.

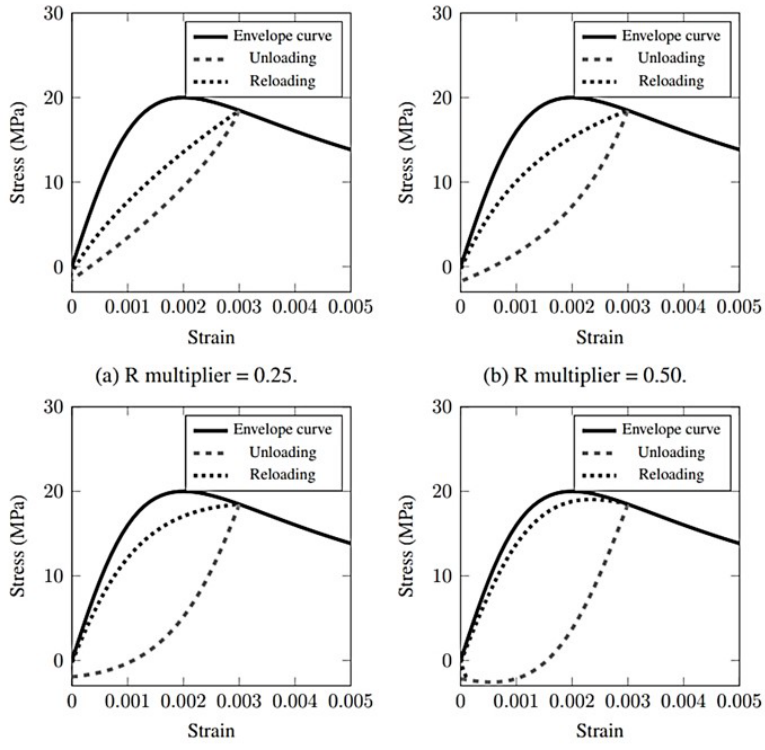

(a) R multiplier = 0.25. (b) R multiplier = 0.50.

(c) R multiplier = 0.75. (d) R multiplier = 1.00.

Figure 7. R multiplier: parameter analysis.

6 NUMERICAL SIMULATIONS

The proposed cyclic smeared crack model was presented in the previous sections, and the linear and nonlinear stress-strain laws were described. Based initially on a fixed focal point, such laws were improved by a moving focal point adaptable to the load cycle representation.

Two numerical simulations were performed to show the improvement made by the new methodology. The first example is an experimental test of direct cyclic tension in plain concrete accomplished by Gopalaratnam and Shah [33], as shown in Figure 8a. The second example (Figure 8b) is a direct cyclic compression investigated experimentally by Karsan and Jirsa [2].

Table 3. Study of the variable Δκ.

Tensile					Compression				
Reference	Cycle	$\varepsilon_u^1(\%)$	$\varepsilon_r^1(\%)$	$\Delta\kappa = \varepsilon_r/\varepsilon_u$	Reference	Cycle	$\varepsilon_u^1(\%)$	$\varepsilon_r^1(\%)$	$\Delta\kappa = \varepsilon_r/\varepsilon_u$
[32]	1	0.128	0.134	1.047	[2] 1st test	1	0.865	1.137	**1.314**[2]
	2	0.186	0.201	1.080		2	1.137	1.407	1.238
	3	0.262	0.278	1.061		3	1.407	1.587	1.128
	4	0.321	0.340	1.059		4	1.966	2.336	1.188
	5	0.393	0.415	1.057		5	2.655	2.942	1.109
[3], [33], [34] 1st test	1	0.011	0.012	1.122	[2] 2nd test	1	0.808	0.981	1.214
	2	0.016	0.020	1.243		2	1.115	1.253	1.124
	3	0.03	0.035	1.099		3	1.378	1.603	1.163
	4	0.044	0.046	1.042		4	1.603	1.854	1.156
	5	0.064	0.070	1.088		5	1.934	2.238	1.158
	6	0.106	0.110	1.034	[30]	1	1.914	2.168	1.133
[3], [33], [34] 2nd test	1	0.007	0.008	1.090		2	2.357	2.756	1.169
	2	0.008	0.008	1.016		3	4.249	4.373	1.030
	3	0.009	0.010	1.074	[31] 1st test	1	1.965	2.141	1.090
	4	0.010	0.012	1.207		2	2.859	3.239	**1.013**[3]
	5	0.014	0.014	1.036		3	3.930	3.239	1.059
	6	0.016	0.017	1.083		4	4.838	4.162	1.086
	7	0.0020	0.023	1.145	[31] 2nd test	1	1.801	1.976	1.097
	8	0.028	0.031	1.086		2	2.518	2.476	1.090
[3], [33], [34] 3rd test	1	0.009	0.001	1.212		3	3.550	3.953	1.113
	2	0.014	0.016	1.125		4	4.399	4.962	1.105
	3	0.019	0.021	1.148		5	5.308	5.920	1.115
	4	0.021	0.023	1.077		6	6.243	6.497	1.041
	5	0.026	0.030	1.126	[32]	1	1.046	1.219	1.165
	6	0.035	0.036	1.044		2	1.614	1.660	1.029
	7	0.048	0.051	1.063		3	2.096	2.388	1.140
	8	0.075	0.077	1.028		4	2.676	2.858	1.068
						5	3.223	3.281	1.018
						6	3.651	3.997	1.095
					[1]	1	0.884	1.147	1.298
						2	1.282	1.501	1.171
						3	1.656	1.878	1.134
						4	1.878	2.052	1.093
						5	2.265	2.477	1.094
						6	2.581	2.753	1.067

[1]estimated values; [2]maximum value; [3]minimum value.

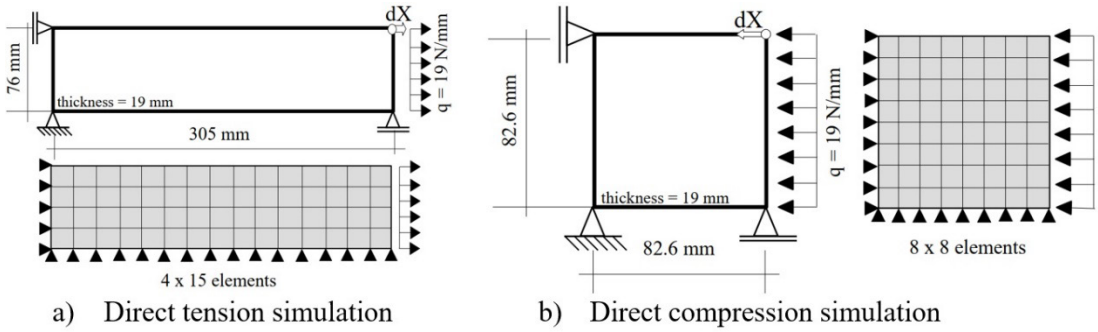

Figure 8. Structural models.

6.1 Cyclic direct tension

Gopalaratnam and Shah [33] conducted experimental tests of cyclic direct tension in plain concrete samples, with prismatic geometry of rectangular base and dimensions of $305 \times 76 \times 19$ mm. The concrete properties were tensile strength $f_t = 3.53$ MPa, the strain that limits the elastic regime $\varepsilon_t = 1.18 \times 10^{-4}$, and fracture energy $G_f = 0.0564$ N/mm.

The numerical analysis was performed using a mesh with 60 four-node quadrilateral finite elements, as illustrated in Figure 8a. This figure also indicates the structural model boundary conditions and highlights the control node. The nonlinear analysis was conducted with the Standard Newton-Raphson method, with the direct displacement control by Batoz and Dhatt [36]. The displacement increment was 5×10^{-8} m on the right superior corner node, as shown in Figure 8a, and the cycles were introduced according to the load limits observed in the experimental data.

The stress-strain laws chosen for the envelope curve were the tensile law from Boone et al. [37] and the compressive law from Carreira and Chu [22]. The Poisson ratio, the concrete compression strength, and its related strain were estimated by $\nu = 0.18$, $f_c = 40.4$ MPa, and $\varepsilon_c = 0.002$. The characteristic length was $h = 166$ mm. The linear (Figure 9) and nonlinear (Figure 10) laws presented in this work were applied for the unloading and reloading regimes.

The linear formulation with fixed focus is presented in Figure 9a, whose implementation was based on the analytical study of Lee et al. [7] and Lee and Willam [8]. The focal point coordinate was established according to Kwon and Spacone [9], coinciding with the concrete compression strength (ε_c, f_c). Considering the limitation of a linear path, the first two cycles were coherent with experimental data regarding the unloading start and permanent strain. On the other hand, the last three cycles started in the expected regions, but their permanent strains were overestimated.

Three other simulations were performed using the moving focal point to minimize this disparity. The first one is illustrated in Figure 9b, using the maximum strain similar to the one verified experimentally, $\varepsilon_{max} = 0.005$. The correction strategies were not required in this simulation. The resulting curve presents relevant improvements in permanent strain representation when compared with Figure 9a. However, the cycles inclination showed a lag of the experimental curve.

A third simulation was conducted. The maximum strain was replaced by $\varepsilon_{max} = 0.004$, coupled with the correction strategy that fixes the permanent strain if it violates physical laws. The results are presented in Figure 9c. All the cycles converged to experimental data except for the last. This discrepancy indicates that the correction strategy was inadequate.

Because of this, a last simulation was accomplished, preserving $\varepsilon_{max} = 0.004$, but replacing the correction strategy for the one that fixes the damaged modulus. The results are available in Figure 9d, which presents an accurate fit with the experimental curve. This simulation emphasizes the improvements the moving focal point can offer to cyclic numerical analyses.

Nevertheless, the linear approach can only represent the cycle location and permanent strain. A nonlinear law is demanded to reproduce the experimental cycle configuration. New simulations were performed using this approach. The first (Figure 10a) refers to the implementation of the law from Popovics-Saenz adapted by Bono and Campos [29]. Some parameters of the Popovics-Saenz law were defined to enable this analysis, such as $k_{ref} = 0.85$ and $\beta_{ref} = 1.80$. The other analyses embrace the proposed concept of the moving focal point.

It can be observed in Figure 10a that since the focus was defined as the concrete compression strength (ε_c, f_c), which is distant from the points where unloading starts, the nonlinear approach was limited to the linear stretch. Because of that, the numerical curve was similar to the ones in Figure 9, and the nonlinear approach could not be well represented.

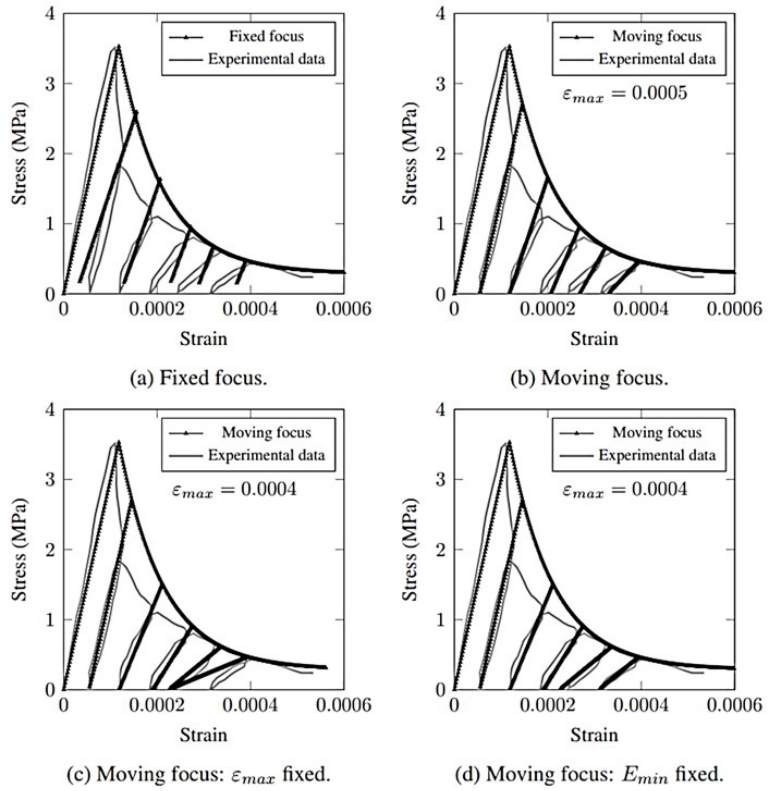

(a) Fixed focus. (b) Moving focus.

(c) Moving focus: ε_{max} fixed. (d) Moving focus: E_{min} fixed.

Figure 9. Tension test with the linear cyclic approach.

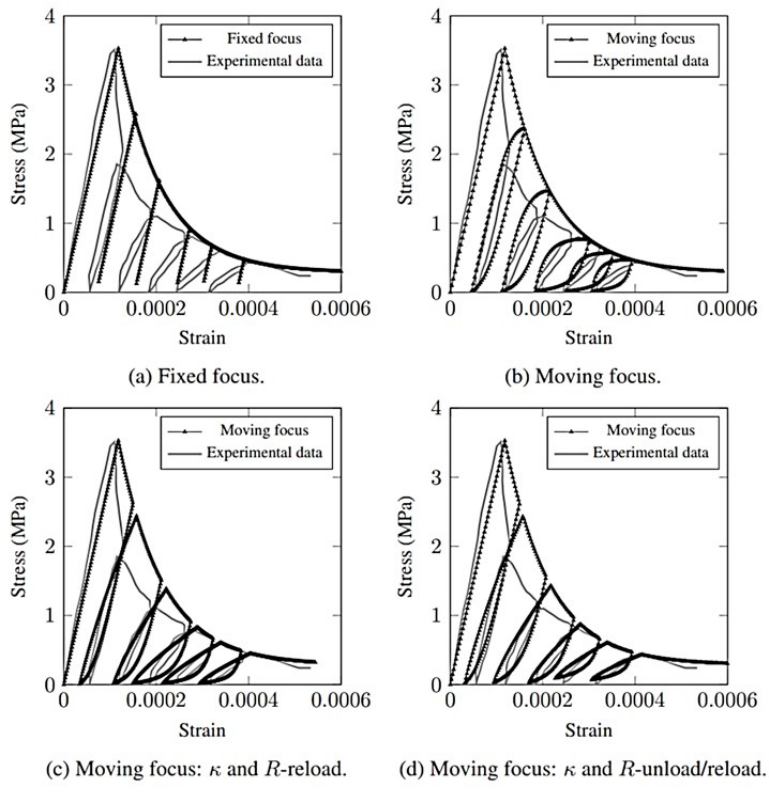

(a) Fixed focus. (b) Moving focus.

(c) Moving focus: κ and R-reload. (d) Moving focus: κ and R-unload/reload.

Figure 10. Tension test with nonlinear cyclic approach.

The same simulation was repeated to include nonlinearity, applying the moving focal point (Figure 10b). The curve fits experimental data describing cycles location and permanent strains. The cycles configuration, however, did not converge with the tests from Gopalaratnam and Shah [33].

Two adjustment parameters were introduced to improve cycles configuration in a third simulation (Figure 10c). The historical variable was incremented between the unloading point and the end of the reloading process in $\Delta\kappa = 1.05$, and the exponent R of the Popovics-Saenz law was multiplied for 0.2 during the reloadings, which minimizes its curvature. After these corrections, the numerical response converges to the experimental curve.

One last improvement was made by multiplying the exponent R by 0.85 in unloading, as presented in Figure 10d. This numerical curve was considered the closest result reached using the nonlinear approach, performing a high fidelity in representing permanent strains and cycles location and configuration.

6.2 Cyclic direct compression

The concrete response was also evaluated under cyclic direction compression. The numerical simulations used the experimental studies of Karsan and Jirsa [2] as a reference. The analyses were performed by adopting a mesh with 64 four-node quadrilateral finite elements, whose geometry, boundary conditions, and node of control are presented in Figure 8b.

The parameters obtained experimentally from Karsan and Jirsa [2] are the Poisson ratio $\nu = 0.18$, the elastic modulus $E = 31700$ MPa, the fracture energy $G_f = 0.04$ N/mm, the concrete compression strength $f_c = 27.6$ MPa, and the characteristic length $h = 82.6$ mm. The other required parameters to the tensile law from Boone et al. [37] and the compression law from Carreira and Chu [22] were defined based on the experimental results, assuming the values: concrete tensile strength $f_t = 2.76$ MPa, and the strain related to concrete compression strength $\varepsilon_c = 0.0016$.

Initially, numerical simulations were accomplished with the linear approach. Similar to the direct tension simulation, a fixed focal point located in the concrete tensile strength (ε_t, f_t) was adopted, as indicated in Figure 11a. The results using this focal point, located near the origin, were similar to secant unloading-reloading, as discussed in Pereira and Penna [15]. Since the cycles are directed to the origin adjacencies, this simulation failed to represent the permanent strains.

To improve the reproduction of the permanent strains, simulations with the moving focal point were performed. The maximum strain was considered as $\varepsilon_{max} = 0.006$, a value slightly superior to the one observed on tests, resulting in the curve illustrated in Figure 11b.

The result was better than the one indicated in Figure 11a, but the permanent strains showed a gap from experimental data.

Then, a new simulation was performed for $\varepsilon_{max} = 0.0055$ coupled with the correction strategy that fixes the permanent strain when this parameter reaches an incoherent value (Figure 11c). An analogous analysis was accomplished, replacing the correction method with the one that fixes the damaged modulus (Figure 11d). Except for the last cycle, the results were similar to the second simulation (Figure 11b). The change of the maximum strain did not conduct improvements. Among the obtained results, the one indicated in Figure 11b was the closest to the experimental curve. Once more, it is highlighted that the linear approach can only estimate the cycle location and the associated permanent strain. A nonlinear approach is needed to reproduce the cycle configuration, especially in compression analyses with strong nonlinearity. Other simulations were performed considering these aspects.

The unloading-reloading laws based on Popovics-Saenz required some extra parameters: β_{ref}, which assume values between 1.70 and 1.75, and $k_{ref} = 0.85$. These parameters were obtained from parametrization to adjust the experimental envelope curve better. The nonlinear approach using Popovics-Saenz laws and a fixed focal point established as the concrete tensile strength (ε_t, f_t) is indicated in Figure 12a.

Compared with the linear approach, improvements were verified in reproducing the permanent strains and the cycle configuration. Although, the cycles location did not fit with the experimental data. This fact can be related to the lack of flexibility in using a unique focus for all cycles. Then, another simulation was conducted, coupling the proposed moving focal point and the nonlinear approach. The cycles positions were corrected, as shown in Figure 12b, but their configurations were wider than the ones observed on tests.

To refine the results, the historical parameter received an increment of $\Delta\kappa = 1.05$ to represent the difference between the unloading start and the reloading end (Figure 12c), according to the experimental curve. However, this intervention did not modify the shape of the cycles. As discussed, the factor responsible for the loop form is the exponent R. Then, a last simulation was realized, including a correction factor for this parameter during the reloading to reduce these stretches curvature, as shown in Figure 12d. Different values of R were admitted to each cycle. The numerical curve finally indicates a good agreement with the experimental data, emphasizing the efficiency of the methodology proposed in this article: the parametrization of a cyclic test can be successfully reached by adopting the moving focal point and some correction parameters.

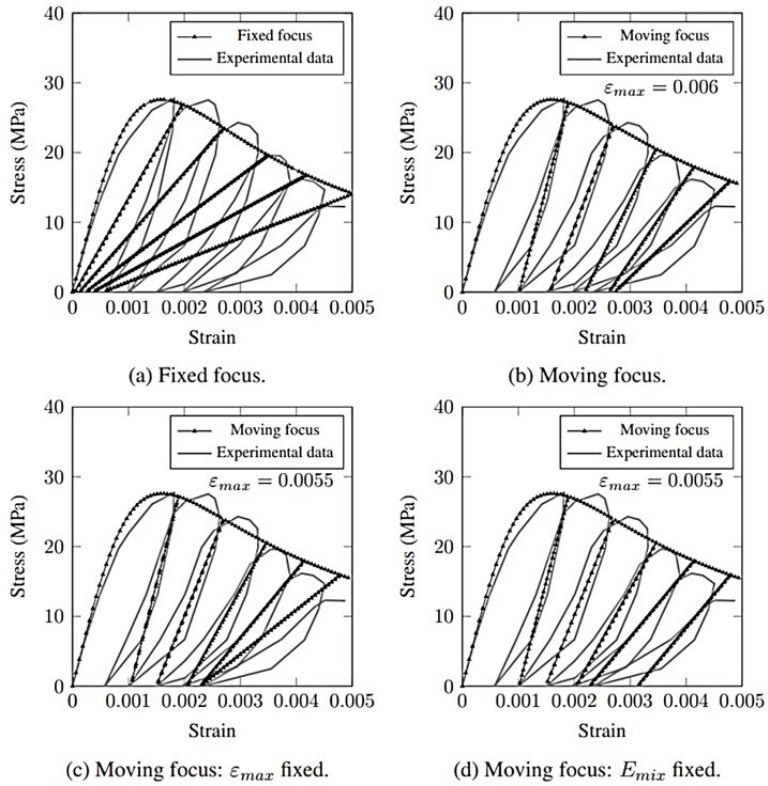

(a) Fixed focus. (b) Moving focus.

(c) Moving focus: ε_{max} fixed. (d) Moving focus: E_{mix} fixed.

Figure 11. Compression test with linear cyclic approach.

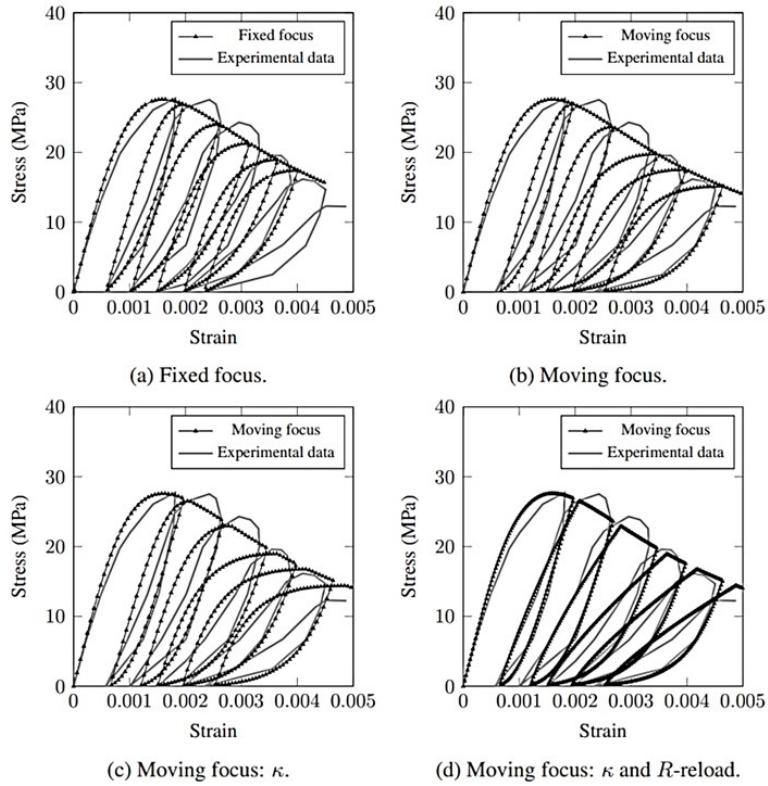

(a) Fixed focus. (b) Moving focus.

(c) Moving focus: κ. (d) Moving focus: κ and R-reload.

Figure 12. Compression test with nonlinear cyclic approach.

6.3 Secant modulus

A last study is presented to show how the secant modulus (E_s) varies with damage evolution in a monotonic and in a cyclic analysis. The tension and compression simulations described in the previous sections are used in this analysis, considering the best results obtained.

First, monotonic simulations were performed for tension and compression (Figures 13a and 13b, respectively), and the envelope curves were determined. Then, the damage evolution was evaluated in the loading direction. Considering the relation in Equation 46, the secant modulus variation could be plotted, as indicated in Figures 13c and 13d.

$$E_s = (1 - D)\, E^0. \tag{46}$$

As expected, the simulations presented a maximum value at the beginning of the analyses that decays according to damage growth. For the tension test, the maximum value is preserved until the damage variable assumes a value higher than zero, indicating that the tension response is elastic until the degradation process starts. In contrast, in the compression test, the nonlinearity is verified since the first steps, and the secant modulus suffers change since the analysis beginning.

The same procedure was applied to the cyclic analyses. The main difference in these cases is the presence of loading cycles. The historical variable remains the same when the structure is under unloading and reloading. Consequently, the damage variable and the secant modulus stand constant. These behaviors can be observed in the graphics of Figure 13.

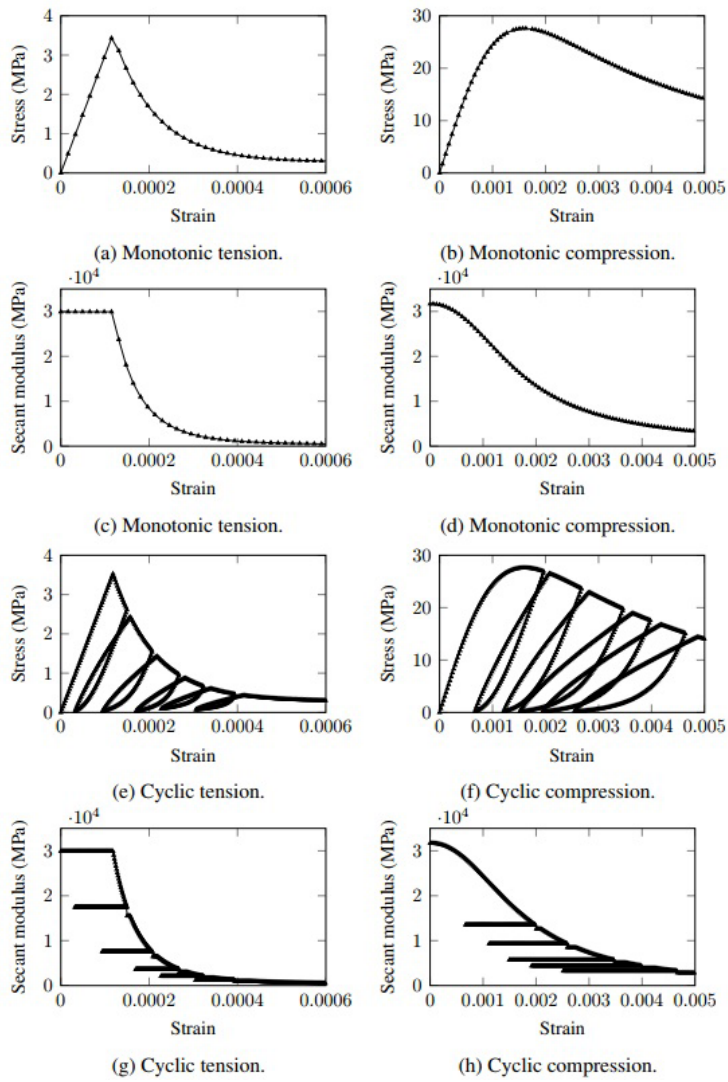

Figure 13. Damage evolution and secant modulus variation.

During the load loops (Figures 13e and 13f), the secant modulus stays unchanged, according to the horizontal lines indicated in Figures 13g and 13h. The shapes of these curves, relating the secant modulus and the current strain, respect the monotonic ones (Figures 13c and 13d), except by the lines from the cycles and the gaps between the unloading and the reloading point, which are justified by the parameter Δκ. Then, the proposed model provides a coherent relation between degradation and cyclic representation.

7 CONCLUSIONS

A material model has been presented based on a smeared crack approach capable of describing the concrete behavior under cyclic loadings in both compression and tension. The model adopts constitutive laws based on a moving focal point, which coordinates changes according to the unloading stress-strain state of concrete. Two approaches are available to represent the load loops: the linear and the nonlinear approach.

Particular emphasis has been given to reproducing three characteristics in cyclic analyses: stiffness degradation, permanent strains, and cycle configuration. Adopting a formulation based on a focus with flexible coordinates ensured the first two characteristics. About the cycle configuration, for tensile loads, the cycles can be satisfactorily approximated by a line. Considering compression solicitations, the cycle nonlinearity becomes more intense, and the nonlinear approach is required.

The proposed methodology includes adjustment variables that proved to be valuable resources. The first is the correction strategies, which prevent results without physical meaning in the linear approach. These strategies are based on the fixation of a degradation parameter, which can be the permanent strain or the damaged modulus. A second quantity is the Δκ, responsible for applying an increment over the historical variable to differentiate the unloading start to the reloading end in the nonlinear approach. Finally, the exponent R of Popovics-Saenz can be multiplied by a modifier to better represent the nonlinear cycles.

The model has been validated by comparing numerical simulations and experimental data available in the literature. The proposed model shows improvements over the fixed focal point model in all cases. Future studies can evaluate the response of the proposed model to more complex cases of cyclic loads.

ACKNOWLEDGEMENTS

The authors gratefully acknowledge the support of the Brazilian research agency CNPq (in Portuguese Conselho Nacional de Desenvolvimento Científico e Tecnlógico) for the PhD Scholarship and the Research Grant n. 307985/2020-2.

REFERENCES

[1] B. P. Sinha, K. H. Gerstle, and L. G. Tulin, "Stress-strain relations for concrete under cyclic loading," *J. Am. Concr. Inst.*, vol. 61, no. 2, pp. 195–211, 1964, http://doi.org/10.14359/7775.

[2] I. D. Karsan and S. O. Jirsa, "Behavior of concrete under compressive loadings," *J. Struct. Div.*, vol. 95, no. 12, pp. 2543–2563, 1969, http://doi.org/10.1061/JSDEAG.0002424.

[3] H. W. Reinhardt, "Fracture mechanics of an elastic softening material like concrete," *Heron*, vol. 29, no. 2, pp. 1–42, 1984.

[4] D. Z. Yankelevsky and H. W. Reinhardt, "Model for cyclic compressive behavior of concrete," *J. Struct. Eng.*, vol. 113, no. 2, pp. 228–240, 1987, http://doi.org/10.1061/(ASCE)0733-9445(1987)113:2(228).

[5] D. Z. Yankelevsky and H. W. Reinhardt, “Focal point model for uniaxial cyclic behavior of concrete,” in *Proc. IABSE Colloq.*, Delft, 1987, pp. 99–106, http://doi.org/10.5169/seals-41920.

[6] D. Z. Yankelevsky and H. W. Reinhardt, "Uniaxial behavior of concrete in cyclic tension," *J. Struct. Eng.*, vol. 115, no. 1, pp. 166–182, 1989, http://doi.org/10.1061/(ASCE)0733-9445(1989)115:1(166).

[7] Y. H. Lee, K. Willam, H. D. Kang, “Experimental observations of concrete behavior under uniaxial compression,” in *Proc. FRAMCOS-2*, 1995, pp. 397–414.

[8] Y. H. Lee and K. Willam, "Mechanical properties of concrete in uniaxial compression," *ACI Mater. J.*, vol. 94, no. 6, pp. 457–471, 1997, http://doi.org/10.14359/329.

[9] M. Kwon and E. Spacone, "Three-dimensional finite element analyses of reinforced concrete columns," *Comput. Struc.*, vol. 80, no. 2, pp. 199–212, 2002, http://doi.org/10.1016/S0045-7949(01)00155-9.

[10] G. M. S. Alva, R. M. F. Canha, J. Oliveira Fo., and A. L. H. C. El Debs, "Numerical model for analysis of reinforced concrete beams under repeated cyclic loads," *Sci. Eng. J.*, vol. 22, no. 2, pp. 105–114, 2013, http://doi.org/10.14393/19834071.2013.23805.

[11] M. Breccolotti, M. F. Bonfigli, A. D’Alessandro, and A. L. Materazzi, "Constitutive modeling of plan concrete subjected to cyclic uniaxial compressive loading," *Constr. Build. Mater.*, vol. 94, pp. 172–180, 2015, http://doi.org/10.1016/j.conbuildmat.2015.06.067.

[12] J. F. Sima, P. Roca, and C. Molins, "Cyclic constitutive model for concrete," *Eng. Struct.*, vol. 30, no. 3, pp. 695–706, 2008, http://doi.org/10.1016/j.engstruct.2007.05.005.

[13] M. Moharrami and I. Koutromanos, "Triaxial constitutive model for concrete undercyclic loading," *J. Struct. Eng.*, vol. 142, no. 7, pp. 1–15, 2016, http://doi.org/10.1061/(ASCE)ST.1943-541X.0001491.

[14] D. C. Feng, Z. Wang, X. Y. Cao, and G. Wu, "Damage mechanics-based modeling approaches for cyclic analysis of precast concrete structures: a comparative study," *Int. J. Damage Mech.*, vol. 29, no. 8, pp. 965–987, 2020, http://doi.org/10.1177/1056789519900783.

[15] L. R. S. Pereira and S. S. Penna, "Nonlinear analysis method of concrete under cyclicloading based on the generalized secant modulus," *Rev. IBRACON Estrut. Mater.*, vol. 15, no. 4, pp. 1–20, 2022, http://doi.org/10.1590/s1983-41952022000400006.

[16] Y. R. Rashid, "Ultimate strength analysis of prestressed concrete pressure vessels," *Nucl. Eng. Des.*, vol. 7, no. 4, pp. 334–344, 1968, http://doi.org/10.1016/0029-5493(68)90066-6.

[17] D. Darwin and D. A. Pecknold, "Analysis of RC shear panels under cyclic loading," *J. Struct. Div.*, vol. 102, no. 2, pp. 355–369, 1976, http://doi.org/10.1061/JSDEAG.0004282.

[18] Z. P. Bažant and B. H. Oh, "Crack band for fracture of concrete," *Materiaux Constructions*, vol. 16, no. 93, pp. 155–177, 1983, http://doi.org/10.1007/BF02486267.

[19] Z. P. Bažant and B. H. Oh, "Deformation of progressively cracking reinforced concretebeams," *J. Am. Concr. Inst.*, vol. 81, no. 3, pp. 268–278, 1984, http://doi.org/10.14359/10683.

[20] J. G. Rots, "Computational modeling of concrete fracture," Ph.D. dissertation, Delft Univ. Technol., Delft, Netherlands, 1988.

[21] J. G. Rots, P. Nauta, G. M. A. Kusters, and J. Blaauwendraad, "Smeared crack approach and fracture localization in concrete," *Heron*, vol. 30, no. 1, pp. 1–48, 1985.

[22] D. J. Carreira and K. H. Chu, "Stress-strain relationship for plain concrete in compression," *J. Am. Concr. Inst.*, vol. 82, no. 6, pp. 797–804, 1985, http://doi.org/10.14359/10390.

[23] T. Boone and A. R. Ingraffea, "Simulation of the fracture process at rock interfaces," in *Proc. 4th Int. Conf. Num. Meth. Frac. Mech.*, 1987, pp. 519–531.

[24] Z. Li and Q. Ren, "Development of a practical uniaxial cyclic constitutive model for concrete," *IOP Conf. Ser.: Earth Environ. Sci.*, vol. 295, pp. 042057, 2019, http://doi.org/10.1088/1755-1315/295/4/042057.

[25] T. A. Balan, F. C. Filippou, and E. P. Popov, "Constitutive model for 3D cyclic analysis ofconcrete structures," *J. Eng. Mech.*, vol. 123, no. 2, pp. 143–153, 1997, http://doi.org/10.1061/(ASCE)0733-9399(1997)123:2(143).

[26] T. A. Balan, E. Spacone, and M. Kwon, "A 3D hypoplastic model for cyclic analysis ofconcrete structures," *Eng. Struct.*, vol. 23, no. 4, pp. 333–342, 2001, http://doi.org/10.1016/S0141-0296(00)00048-1.

[27] S. A. Popovics, "A numerical approach to the complete stress-strain curve of concrete," *Cement Concr. Res.*, vol. 3, no. 5, pp. 583–599, 1973, http://doi.org/10.1016/0008-8846(73)90096-3.

[28] L. P. Saenz, "Discussion of equation for the stress-strain curves for concrete by Desai, P. and Krishnan, S.," *ACI J.*, vol. 61, no. 9, pp. 1229–1235, 1964.

[29] G. F. F. Bono and A. Campos Fo., "Simulação numérica tridimensional em peças de concreto armado através do método dos elementos finitos," *Mec. Computacionalvol.*, vol. 28, pp. 1715–1730, 2009.

[30] D. C. Spooner and J. W. Dougill, "A qualitative assessment of damage sustained in concrete during compressive loading," *Mag. Concr. Res.*, vol. 27, no. 9, pp. 151–160, 1975, http://doi.org/10.1680/macr.1975.27.92.151.

[31] S. Okamoto, S. Shiomi, and K. Yamabe, "Earthquake resistance of pre-stressed concrete structures," in *Proc. Ann. Conv. AIJ*, 1976, pp. 1251–1252.

[32] Y. Tanigawa and Y. Uchida, "Hysteretic characteristics of concrete in the domain of high compressive strain," in *Proc. Ann. Conv. AIJ*, 1979, pp. 449–450.

[33] V. Gopalaratnam and S. Shah, "Softening response of plain concrete in direct tension," *J. Am. Concr. Inst.*, vol. 82, no. 3, pp. 310–323, 1985, http://doi.org/10.14359/10338.

[34] J. M. Moelands, "Modelling of fatigue behavior of plain concrete under alternating and repeated loading," Ph.D. dissertation, Delft Univ., Delft, Netherlands, 1984.

[35] H. A. W. Cornelissen, D. A. Hordijk, and H. W. Reinhardt, "Experiments and theory for the application of fracture mechanics to normal and lightweight concrete," in *Fracture Toughness and Fracture Energy of Concrete*, F. H. Wittmann, Ed., Amsterdam: Elsevier, 1986, pp. 565–575.

[36] J. L. Batoz and G. Dhatt, "Incremental displacement algorithms for nonlinear problems," *Int. J. Numer. Methods Eng.*, vol. 14, no. 8, pp. 1262–1267, 1979, http://doi.org/10.1002/nme.1620140811.

[37] T. J. Boone, P. A. Wawrzynek, and A. R. Ingraffea, "Simulation of the fracture process at rock with application to hydrofracturing," *Int. J. Rock Mech. Min. Sci. Geomech. Abstr.*, vol. 23, no. 3, pp. 255–265, 1986, http://doi.org/10.1016/0148-9062(86)90971-X.

Author contributions: LRSP: conceptualization, formal analysis, methodology, writing; SSP: conceptualization, methodology, writing, supervision.

Editors: Samir Maghous, Daniel Carlos Taissum Cardoso.